RSC Advances

ROYAL SOCIETY OF CHEMISTRY

www.rsc.org/advances

An in-vitro cytotoxicity study of 5-Fluorouracil encapsulated chitosan/gold nanocomposite towards MCF-7 cells

E A K Nivethaa[a], S. Dhanavel[a], V Narayanan [b], C. Arul Vasu[c] and A Stephen[a,*]

[a]*Material Science Centre, Department of Nuclear Physics, University of Madras, Guindy Campus, Chennai-25, India.*
[b]*Department of Inorganic Chemistry, University of Madras, Guindy Campus, Chennai 600 025, India.*
[c]*Department of Zoology, University of Madras, Guindy Campus, Chennai 600 025, India.*

**E-mail: stephen_arum@hotmail.com*
Phone: 044-22202802, Fax. 044-22351269

Abstract

Chitosan/gold nanocomposite was synthesized using chemical reduction method. XRD pattern shows the semi-crystalline nature of chitosan and the face centered cubic structure of gold. Binding of gold to chitosan was confirmed using XPS and FTIR. The presence of gold in its metallic state is evident from XPS. The prepared nanocomposite was used as a drug delivery carrier for 5-Fluorouracil. The encapsulation efficiency of 5-FU and the drug loading efficiency were found to be 96% and 41% respectively. A dialysis membrane was used to study the release of 5-Fluorouracil from chitosan/gold nanocomposite. The amount of drug released in-vitro was analyzed using the UV-vis characterization of PBS solution. 5-Fluorouracil encapsulated nanocomposite was characterized using HRTEM with SAED, HRSEM with elemental mapping, XRD and FTIR analysis. The presence of fluorine, observed from the elemental mapping confirms the loading of drug into the nanocomposite. Cytotoxicity analysis was performed for the MCF-7 and VERO cell lines, which shows the effectiveness of the sample towards the destruction of MCF-7 and its non-toxicity towards the VERO. 50% cell viability for the MCF-7 cells was obtained at a sample concentration of 31.2 μg/ml. The non-toxicity of the system towards VERO cells at the concentration wherein IC_{50} is obtained for MCF-7 and the adherence of the maximum portion of the release profile to zero order kinetics, which means a constant release of the drug from the delivery vehicle are the highlights of this system.

Keywords: Chitosan, gold, Nanocomposite, Drug release, Cytotoxicity.

1. Introduction

The use of nanoparticles in the biological field has increased due to the superior properties that they possess when compared to their bulk counterparts such as enhanced permeability and retention and the ease with which they are taken up by the cells as demonstrated by Y. Liu et al. in the use of nanovectors for gene delivery and K. Siegrist et al. for the case of low density carbon nanotubes [1, 2]. Apart from this, nanoparticles own a functional surface which gives the nanoparticles the ability to bind, adsorb and carry other compounds thus, making them suitable for drug delivery[3-5]. Besides this , the nanoparticles also protect the drug from degradation, enable a prolonged release of the drug, improve the bioavailability of the drug, reduce the toxic side effects of the drug and offer an appropriate form for all routes of administration[6].

Of these nanoparticles, noble metal nanoparticles are preferred due to their optical properties[7], non toxicity and biocompatibility[8] when compared to the other metals . Majorly, gold nanoparticles can convert light or radio frequency into heat thus enabling the thermal ablation of the targeted cancer cells. This type of phenomenon has been observed for gold nanoparticles by T. Nikunj et al.. and R. James et al. [9, 10]. Hence, the ability to combine drug delivery and photothermal therapy on gold nanoparticle based delivery platforms prove it to be a system that is capable of eliminating the cancer cells. One major drawback that arises while using gold nanoparticles, is its agglomeration during reduction from its metal salts. Takami Shimizu et al.. has reported the importance of the control of nanoparticle size [11] as the increased particle size reduces the scope for their use in drug delivery since it is well known that particles with size ranging from 10 to 50 nm are the ones that are easily taken up by the cells. Thus, an effective way to prevent the aggregation of gold nanoparticles is mandatory. An effective strategy for this would be the use of a stabilizing agent or surfactant[12-14]. The most promising and environment friendly stabilizing agents are enzymes [15] and polymers [16, 17].

The role of a stabilizing agent/surfactant is played by a chitosan[18]. Chitosan is a biopolymer that is biocompatible, biodegradable, ecofriendly, non-toxic and has NH_2 and OH groups which act as chelating sites for drugs (5-Fluorouracil in our case) and for other molecules[19-23]. Moreover, as the combination of nanoparticles with chitosan in the form of nanocomposite matrices provide the high surface area required to achieve a high loading of enzymes, drugs, and a compatible micro-environment to facilitate stability as reported by Jay Singh et al.., chitosan is suitable for use as a drug delivery carrier [8]. There are a number of

reports on the use of gold nanoparticles and chitosan separately for drug delivery [24, 25]. A nanocomposite system consisting of both gold and chitosan will encompass the properties of both the moieties, which makes it a powerful choice for use in the biocompatible, targeted delivery and sustained release of 5-Fluorouracil (5-FU).

5-FU is an anticancer drug with a broad activity against solid tumors, alone or in combination with chemotherapy. It comes under the class of cytotoxic anticancer drugs that pose harmful side effects by attacking both healthy and cancerous cells, which has inhibited its use in spite of its effectiveness towards the destruction of cancer cells[26]. The use of 5-FU for the treatment of breast cancer is prevalent. To the best of our knowledge there are no reports on the cytotoxicity behavior of 5-Fluorouracil loaded chitosan/gold nanocomposite towards MCF-7 cell line. Thus, in the present work encapsulation of 5-FU into chitosan/gold (CS/Au) nanocomposite has been tried, to improve the biocompatibility of 5-FU and to test the cytotoxicity of the nanocomposite towards the breast cancer cell line. CS-Au nanocomposite with and without drug encapsulation has been prepared. The prepared nanocomposite has been characterized using various techniques like XRD, FTIR, HRTEM, XPS and UV. In-vitro drug release studies have been performed using an UV spectrophotometer after the encapsulation of 5-FU into the composite. Cytotoxicity of 5-FU encapsulated nanocomposite towards the MCF-7 and VERO cell lines have also been studied.

2. Materials and Methods

2.1 Materials

Chitosan (CS) from Sigma Aldrich (low molecular weight and ~85% deacetylated), gold chloride ($HAuCl_4$) with ~50% Au basis and 5-Fluorouracil with ≥ 99% purity from Sigma Aldrich, sodium tripolyphosphate (TPP) 98% pure from Alfa Aesar, Tween 80, ultra pure from Alfa Aesar and sodium borohydride ($NaBH_4$) extrapure 99% purity from Finar reagents were used for synthesis. Dimethyl sulfoxide (DMSO) with ≥ 99% purity was purchased from Sigma Aldrich. All chemicals used were of analytical grade. All experiments were carried out using double distilled water.

2.2 Preparation of chitosan-gold polymer matrix nanocomposite

Chitosan/gold (CS-Au) nanocomposite was prepared using a simple and cost effective chemical method. In this method gold nanoparticles were obtained by the in situ reduction of

gold chloride in a solution of chitosan. Composite containing 5, 10 and 15 weight percentage of gold were synthesized using the procedure mentioned below and characterized.

Chitosan was dissolved in 2% acetic acid (98 ml water + 2ml acetic acid) to obtain a polymer solution at a concentration of 0.34% (w/v). The amount of gold chloride was chosen in such a way that the composite would contain 5% (w/w) gold i.e 0.01728 M solution was taken and added to the chitosan solution kept under simultaneous stirring and sonication. The pH of the solution was found to be ~2. The reduction of gold chloride to gold was accomplished by the dropwise addition of 0.17 M sodium borohydride to the above solution. The pH of the final solution was found to be between 5 and 6. The solution was maintained under stirring and sonication for 2 hrs. The obtained product was washed several times using deionised water to remove the undue sodium borohydride. The solution was centrifuged and the particles were collected and characterized[27].

2.3 Protocol for the synthesis of 5-FU encapsulated chitosan/gold nanocomposite

Chitosan was dissolved in 2% acetic acid solution to maintain chitosan concentration at 0.75 (mg/mL). Prepared chitosan solutions were mixed with 3.8 mM 5-FU solutions (5-FU dissolved in water). Tween 80 (0.5% (v/v)) was added to the above solution, and the pH was maintained between 4.6 and 4.8. Prepared 5-FU-containing chitosan solutions were mixed with 1.4 mM TPP solutions such that ratio of chitosan to TPP is (2: 1) (v/v). The nanoparticle suspension was gently stirred for 180 min at room temperature to allow 5-FU adsorption on the nanoparticles. A solution of gold chloride such that the amount of gold after the reduction of $HAuCl_4$ would be 5% (w/w) gold i.e., 0.019 M gold chloride solution was added to the above solution. A 0.19 M solution of sodium borohydride was added dropwise to the above solution to accomplish the reduction of $HAuCl_4$ to Au. A solution of 5-FU encapsulated chitosan/gold nanocomposite thus obtained was centrifuged, resuspended in water, freeze-dried and the powder obtained was used for further analysis. A scheme representing the synthesis of 5-FU loaded nanocomposite is shown in figure 1.

The X-Ray diffraction analysis of the prepared sample was done using GE X-ray diffraction system-XRD 3003 TT with $CuK\alpha_1$ radiation of wavelength 1.5406 Å. The X-ray photoelectron spectroscopy (XPS) measurement was done using DAR400-XM 1000 (OMICRON Nanotechnologies, Germany) equipped with dual Al/Mg anodes as the X-ray source. The Al anode was used to attain the survey and elemental spectra. All spectra were

calibrated using C 1s peak at 284.5 eV to exclude the charging effect on the sample. HRTEM was carried out using Tecnai instrument operating at 200 kV, equipped with EDAX and SAED facilities. The FTIR spectrum was recorded using Perkin-Elmer FTIR system and Cary 5E UV-VIS-NIR instrument was used for recording the UV spectrum at room temperature using a double beam. The zeta potential was determined using the Zetasizer 300 HAS (Malvern Instruments, Malvern, UK).

3. Results and Discussion

3.1 Structural Investigation

The X-ray diffraction (XRD) pattern of the nanocomposite with and without 5-FU are given in figure 2. The XRD pattern of the nanocomposite containing different weight percentages of gold (fig 2 (a-b)) are almost similar. All the patterns show the presence of chitosan (2ɵ ~ 11.8º and 21º) as well as gold confirming the formation of the nanocomposite. The semi-crystalline nature of chitosan and the face centered cubic (fcc) structure of gold are evident from the XRD pattern. The peaks of gold (2ɵ = 38.1º, 44.4º and 64.5º) are in good agreement with the JCPDS card No. 04-0784[28, 29]. The average crystallite size of gold nanoparticles as calculated using Scherrer's formula is ~ 5nm. The XRD pattern of 5-FU encapsulated chitosan/gold nanocomposite is shown in figure 2c. Peaks corresponding to 5-FU are observed in addition to the peaks of chitosan and gold, affirming the encapsulation of 5-FU to the nanocomposite. The peaks of 5-FU concurred well with the JCPDS card no. 39-1860.

3.2 FTIR Analysis

The FTIR spectrum of CS/Au nanocomposite (figure 3) exhibits a NH_2 twisting peak at ~ 898 cm^{-1}, C-O stretching at ~ 1070 cm^{-1}, C-O-C stretching at ~ 1260 cm^{-1}, C-N stretching at ~ 1318 cm^{-1},C-H bending at 1382 cm^{-1}, CH_2 bending at ~ 1416 cm^{-1}, a peak of NH_3^+ at ~1568 cm^{-1}, C=O stretching and N-H bending at ~1655 cm^{-1}, C-H stretching at~ 2390 $cm^{-1}$and N-H, O-H stretching at ~3400 cm^{-1}.These peaks correspond well to the peaks of pure chitosan except for minor differences that establish the formation of the nanocomposite [30, 31]. The splitting of the NH_3^+ and NH_2 peak increases on increasing the amount of gold in the nanocomposite. This is because of the neutralization of the protonated amine group. An enhancement in the intensity of the NH_2 peak on increasing the amount of gold is an indication of the increase in the percentage of gold, incorporated into the nanocomposite[32, 33]. The FTIR spectrum of 5-FU encapsulated

nanocomposite is shown in figure 4. This pattern shows the presence of a peak at ~740 cm^{-1} corresponding to the C-H out of plane vibration of CF=CH in addition to the peaks observed for the nanocomposite. An enhancement in the intensity of the N-H bending at ~1655cm^{-1} and a shift of the O-H and N-H stretching and a shift from ~ 3400 cm^{-1} to ~ 3456 $cm^{-1}$is observed. All these observations show the encapsulation of 5-FU to CS/Au nanocomposite[34].

3.3 UV- Vis Studies

The UV-Vis spectra taken for the composite containing different weight percentages of gold is shown in figure 5.The UV-VIS spectra for the formation of gold nanoparticles was monitored and obtained after 120 minutes of addition of $NaBH_4$. A single peak corresponding to the surface plasmon resonance of gold was observed in the wavelength range 522-525 nm[35]. A peak in this range is generally attributed to the surface plasmon excitation of small spherical gold nanoparticles. Damped nature of the peak is indicative of the small particle size. In small particles, the mean free path of the electrons is reduced which eventually leads to the peak dampening. The intensity of the peak increased with concentration of gold which implies that the amount of gold binding to chitosan increased.[35, 36].

3.4 Morphology elemental mapping and SAED studies

The HRTEM image of CS/Au nanocomposite is shown in figure 6(a-f). The formation of a polymer matrix type nanocomposite with chitosan as the matrix phase and gold as the filler phase is evident from figure 6(a). The particle size as measured from the image is ~5 nm which is in good agreement with the XRD results and also supports the UV results. Figure 6(b) and 6(c) show the image of the composite at a resolution of 2 nm wherein the fringes in the nanoparticle are visible. The d spacing values as obtained from these images are 0.235 nm and 0.203 nm which correspond to the (111) and (200) planes of the gold nanoparticles. This confirms that the black colored particles observed in the image are gold. The HRTEM images of 5-FU encapsulated CS/Au nanocomposite are shown in figure 6(d) and 6(e). An increase in the particle size to about 11 nm after the encapsulation of 5-FU is observed from the HRTEM images. Agglomeration of nanoparticles are also observed which is an indication of the binding of one 5-FU to more than one chitosan capped gold nanoparticle thus, bringing them closer to one another. This is evident from the elemental mapping shown in figure 6(f). The pink color dots represent gold and the yellow ones represent 5-FU. The SAED pattern of CS/Au nanocomposite and 5-FU encapsulated CS/Au nanocomposite are shown in figure 7(a) and 7(b)

respectively. For the nanocomposite system d spacing values calculated from the pattern correspond to the (200), (220), (400), and (511) planes of gold whereas the SAED pattern of the 5-FU encapsulated nanocomposite apart from the planes of gold diffraction planes of 5-Fu are also observed. The (-1 2 1), (-3 1 4), (1 -6 2) planes of 5-FU are also observed in addition to the (200), (220), (311), (400) and (331) diffractions of gold. The lattice constants calculated using the obtained d spacing values for gold are a=b=c= 4.10 Å for both CS/Au nanocomposite and 5-FU encapsulated CS/Au nanocomposite.

3.5 X-ray Photoelectron Spectroscopy

Figure 8(a) shows the XPS survey spectra of chitosan/gold nanocomposite. The presence of carbon, nitrogen, oxygen and gold in the nanocomposite and the absence of other elements are evident from the survey spectrum. Charge correction was made with carbon as the reference. The C 1s spectra (figure 8(b)) consists of 3 peaks corresponding to the C-C/C-H (284.6 eV), C-N (285.5 eV) and C=O (288.3 eV) environments respectively. The N 1s spectrum (figure 8(c)) was deconvoluted into two peaks, one corresponding to NH_2 (399.3 eV) and the other to NH_3^+ (400.9 eV) respectively. The occurrence of NH_3^+ is due to the protonation of amine groups of chitosan on dissolving it in a solution of 2% acetic acid. A shift of the NH_2 and NH_3^+ peaks by 0.3 eV and 0.9 eV when compared to pure chitosan is a confirmation of the binding of Au to NH_2 groups of chitosan (by the formation of R-NH_2-Au as shown by the equations given below) as observed for the case of adsorption of Cu^{2+} onto chitosan/sargassum composite [37] and to the adsorption of congo red onto chitosan [38].

$$R\text{-}NH_2 + Au \longrightarrow R\text{-}NH_2\text{–}Au \quad (1)$$

$$R\text{-}NH_3^+ + Au \longrightarrow R\text{-}NH_2\text{-}Au + H^+ \quad (2)$$

The O 1s spectrum (figure 8(d)) was deconvoluted into two peaks at binding energies 533.4 eV and 535.1 eV corresponding to OH environment and oxygen atoms in carboxyl groups respectively[39-41]. The role of OH groups of chitosan as active sites is well known. But the absence of shift in the binding energy of OH peak was observed (when compared to pure chitosan). Thus the atomic concentration percentage of OH was calculated for pure chitosan as well as the composite inorder to verify the binding of Au to OH groups of chitosan. The atomic

concentration of OH groups was found to be 85% in the case of pure chitosan and 40% in the case of composite.

The reduction in the atomic concentration percentage may be due to the binding of Au to OH groups of chitosan which is similar to the case of ethylenediamine functionalized carbon nanotubes[42] and chitosan – iron (II, III) complex[41] showing that the reduction here may be correlated to the binding of Au to OH groups of chitosan. The absence of shift in the OH peaks indicates that NH_2 groups of chitosan serve as a more favorable active site for the binding of Au which can be attributed to the easy donation of lone pair of electrons from nitrogen thus leading to the formation of a stable metal complex. The case of NH_2 acting as the major binding site, supporting the present results have already been reported for the adsorption of Cd^{2+} [1, 43, 44].

The gold spectrum (figure 8(e)) shows the presence of both $4f_{7/2}$ (83.8 eV) and $4f_{5/2}$ (87.4 eV) peaks separated by 3.6 eV which is the characteristic of metallic gold. Apart from this the gold spectrum was deconvoluted into two more peaks (85.2 eV and 88.9 eV), separated by a binding energy of 3.6 eV. These peaks also belong to the Au^0 state of gold, but are shifted from the original binding energy values of metallic gold by 1.4 eV. This shift in binding energy towards a higher value is due to the binding of gold[45] nanoparticles to chitosan and also due to the particle size effect[46]. Thus, the binding of gold to chitosan via the NH_2 and OH groups is evident from the XPS analysis.

3.6 Zeta potential analysis

The stability of colloidal aqueous dispersions can be predicted by measuring the zeta potential. The magnitude of the measured zeta potential is an indication of the repulsive force that is present and can be used to predict the long-term stability of the nanoparticle. The zeta potential (figure 9) value of the chitosan/Au nanocomposite is determined by the charge ratio between chitosan and the gold nanoparticles. The obtained zeta potential for the nanocomposite was 87.8 mV, which suggest the highly stable nature of prepared nanoparticles. In the absence of chitosan the zeta potential of -33 mV is reported for the gold nanoparticles by R. Prado-Gotor[47]. The obtained value of +87.8 mV in the case of chitosan/gold nanocomposite is indicative of the relatively strong binding of gold to chitosan. A shift from negative zeta potential value (case of gold alone) to a highly positive value (nanocomposite) is an evidence of the association of chitosan molecules to the gold surface. [48, 49]

3.7 Evaluation of 5-FU encapsulation and loading

Encapsulation efficiency of 5-FU was calculated using the formula below

$$\textbf{Encapsulation efficiency} = \frac{\textbf{(total 5FU – free 5FU)}}{\textbf{(total 5FU)}} \textbf{X100} \quad (3)$$

$$\textit{Drug loading efficiency} = \frac{\textit{(total 5FU – free 5FU)}}{\textit{(weight of 5FU loaded nanocomposite taken)}} \textit{X100} \quad (4)$$

The amount of free 5-FU was obtained from the supernatant solution collected during the centrifugation of the nanoparticles (nanocomposite with 5-FU). An absorbance spectrum of the collected supernatant was obtained from which the amount of 5-FU in the supernatant was calculated. The encapsulation efficiency of 5-FU into CS/Au nanocomposite thus estimated was 96%.The loading efficiency of 5-FU on CS/Au nanocomposite system was also calculated and it was found to be 41%[50]. The values of loading efficiency are higher when compared to the case for 5-FU loaded N,O–Carboxymethyl chitosan nanoparticles[51] as well as 5-FU loaded chitosan-gold nanocomposite synthesized by Parvathy R. Chandran et al.[25, 52]

3.8 5-FU release studies

The release study of 5-FU was performed in a PBS solution of pH ~ 5. It is well known that the cancerous cells have a lower and acidic pH when compared to the normal cells.[53-55] Apart from this, Seda tigli Aylin et al..[25] and Parvathi R. Chandran et al.. [52] report a fast and continuos release of 5-FU at a pH~5 due to the gel-sol transition that takes place releasing the drug. CS/Au gold nanocomposite prepared with known amount of 5-FU (5mg/ml) was suspended in 2 ml phosphate buffer saline, which was then transferred into a dialysis bag (MWCO 1000 Da). The ends of the dialysis bag were sealed and this was kept immersed into a 60 ml phosphate buffer solution maintained under constant stirring. The amount of 5-FU released was determined through the spectrophotometric investigation of 3ml of solution collected at chosen time intervals from the 60 ml solution of phosphate buffer saline into which the dialysis

bag is kept immersed. Same amount of fresh buffer solution was replaced into the beaker immediately after the collection of solution for analysis

A calibration graph (shown in the inset of figure 10 (a)) was plotted to calculate the amount of 5-FU, from the obtained absorbance. For this, known amount of 5-FU (starting with 500 μg/ml) was suspended in phosphate buffer saline (concentration of the solution is known) and the remaining concentrations were obtained by the serial dilution of this solution. Concentration range was chosen to fit the absorbance obtained during the release. The release profile of 5-FU from the nanocomposite system is shown in figure 10(a). Release of 5-FUshows two-phase pattern one upto 40 h and the next upto 72 h. No initial burst release was observed, instead a slow, sustained and prolonged release was observed during the first phase and a sudden burst release was observed during the second phase[56-58]. In order to understand the kinetics and mechanism of drug release the obtained data was fitted to the various mathematical models (zero order, first order, Higuchi, Hixson-Crowell and Korsmeyer-Peppas). According to the correlation values obtained after fitting the data into the various models, the data in the first two regions (region 1: 1 to 6 h and region 2: 10 to 40 h) of the release profile fitted well to the zero order release kinetics which refers to the constant release of drug from a drug delivery device. It has already been reported that this method is the ideal method of drug release in order to achieve a pharmacological prolonged action. Thus the adherence of the first phase of the obtained release profile to this kinetics shows the capability of the nanocomposite system as a good drug delivery system. The diffusion exponent value obtained by fitting Korsmeyer-Peppas kinetics to these regions are about 0.42 and 0.24 for the first and the second regions respectively which confirm that fickian diffusion is the process controlling the release of the drug in these regions. The third region of the release profile fitted well to Higuchi model which describes the drug release as a diffusion process based on the Fick's law. The diffusion exponent for this region found using Korsmeyer-Peppas model has a value of 1.8 which shows super case II transport to be the phenomenon controlling the drug release in this particular phase. Super case II transport is the drug release by both diffusion and the relaxation of polymer chain.

3.9 In-vitro Cytotoxicity Analysis

3.9.1 Cell lines and culture conditions

Human breast cancer cell line MCF-7 and normal cell line VERO were obtained from National centre for cell sciences Pune (NCCS). The cells were maintained in Minimal Essential

Media supplemented with 10% FBS, penicillin (100 U/ml), and streptomycin (100 µg/ml) in a humidified atmosphere of 50 µg/ml CO_2 at 37 °C.

3.9.2 Cytotoxicity Assay

Cytotoxicity of chitosan/gold nanocomposite towards MCF-7 and VERO cell lines was investigated using MTT assay (3-(4, 5-dimethyl-2-thiazolyl)-2, 5-diphenyl-tetrazolium bromide). Cells (1×10^5/well) were plated in 96-well plates and incubated in a 5% CO_2incubator for 72 h. The cells were then treated with 5-FU encapsulated CS/Au nanocomposite of various concentrations in 0.1% DMSO for 24h. Untreated cells were used as control. Later, the samples were removed, washed with phosphate-buffered saline (pH~7.4) and incubated with 20 µl/well (5 mg/ml) MTT dye for another 4 h followed by the addition of 1 ml of DMSO. Viable cells were determined by measuring the absorbance at 540nm. Measurements were performed and the concentration required for a 50% inhibition of viability (IC_{50}) was determined graphically. The effect of the samples on the proliferation of **MCF-7 & VERO** cells was expressed as the % cell viability, using the following formula:

$$\% \text{ cell viability} = \frac{(A540 \text{ of treated cells})}{(A540 \text{ of control cells})} X\ 100 \qquad (5)$$

3.9.3 Cytotoxicity

Figure 10(b) shows the result of cytotoxicity measurement obtained for the MCF 7 cell lines, performed 24 h after the addition of 5-FU encapsulated CS/Au nanocomposite. The drug encapsulated nanocomposite system exhibits a concentration dependent loss of viability. The estimated half maximal inhibitory concentration (IC_{50}) value was found to be 31.2 µg/ml. In order to investigate the cytotoxicity of the samples towards the normal cells cytotoxic measurements were performed for the VERO cells the result of which is shown as an inset of figure 8. The cell viability at 31.2 µg/ml for the VERO cells was found to be 80.1% which clearly shows that the sample does not harm the normal cells [52]. Thus it is evident that the sample exhibits good antiproliferative activity towards MCF-7 cells while being non-toxic to the surrounding non-carcinogenic cells.

4. Conclusion

Chitosan/gold nanocomposite was successfully prepared using the chemical reduction method. The formation of the nanocomposite by the binding of Au to the NH_2 and OH groups of chitosan is evident from the FTIR and XPS analysis. The presence of chitosan in the semi-crystalline state and the formation of face centered cubic gold nanoparticles of ~5nm in size is apparent from XRD and HRTEM. The increase in the amount of gold in the nanocomposite on increasing the amount of gold chloride taken is evident from UV analysis. Apart from this 5-FU encapsulated nanocomposite was also successfully prepared and the encapsulation of 5-FU to the nanocomposite was confirmed using elemental mapping and SAED analysis. Agglomeration of particles on 5-FU encapsulation is observed which indicate the binding of one 5-FU to more than one chitosan stabilized gold nanoparticle. The encapsulation and loading efficiency of 5-FU were calculated and found to be 96% and 41% respectively. Two different release kinetics were observed for the different regions of the profile namely zero order and Higuchi kinetics and the mechanism of release has also been studied which clearly illustrate the capability of the nanocomposite as a system for the sustained and prolonged release of 5-FU. The cytotoxicity analysis of 5-FU encapsulated nanocomposite towards MCF-7 and VERO cell lines clearly shows the effectiveness of the sample in inhibiting the growth of the carcinogenic MCF-7 cells and its non-toxicity towards the non-carcinogenic VERO cells.

Acknowledgement

Author (E.A.K.N) acknowledges DST PURSE for its financial support in the form of fellowship. The National center for nanoscience and nanotechnology, University of Madras is acknowledged for the FESEM, HRTEM and XPS facilities. SAIF, IIT Madras is acknowledged for the FTIR and UV-VIS characterizations. MSRC, IIT Madras is acknowledged for the HRTEM and EDAX analysis.

References

1 Y. Liu, J. Rohrs and P. Wang, *Nano LIFE*, 2014, **04**, 1441007.

2 K. Siegrist, S. Reynolds, M. Kashon, D. Lowry, C. Dong, A. Hubbs, S.-H. Young, J. Salisbury, D. Porter, S. Benkovic, M. McCawley, M. Keane, J. Mastovich, K. Bunker, L. Cena, M. Sparrow, J. Sturgeon, C. Dinu and L. Sargent, *Particle and Fibre Toxicology*, 2014, **11**, 6.

3 H. Xiao, R. Qi, S. Liu, X. Hu, T. Duan, Y. Zheng, Y. Huang and X. Jing, *Biomaterials*, 2011, **32**, 7732.

4 H. Xiao, L. Yan, Y. Zhang, R. Qi, W. Li, R. Wang, S. Liu, Y. Huang, Y. Li and X. Jing, *Chem. Commun.*, 2012, **48**, 10730.

5 H. Xiao, H. Song, Q. Yang, H. Cai, R. Qi, L. Yan, S. Liu, Y. Zheng, Y. Huang, T. Liu and X. Jing, *Biomaterials*, 2012, **33**, 6507.

6 S. Mohanty and P. K. Boga, *International Journal of Research in Pharmaceutical and Biomedical Sciences*, 2010, **1**, 41.

7 S. Lokina, A. Stephen, V. Kaviyarasan, C. Arulvasu and V. Narayanan, *Eur J Med Chem*, 2014, **76**, 256.

8 J. Singh, P. Khanra, T. Kuila, M. Srivastava, A. K. Das, N. H. Kim, B. J. Jung, D. Y. Kim, S. H. Lee, D. W. Lee, D.-G. Kim and J. H. Lee, *Process Biochem*, 2013, **48**, 1724.

9 T. Nikunj, P. Niket, U. M. Upadhyay and S. Viral, *Pharmacie globale international journal of comprehensive pharmacy*, 2012, **2**, 1.

10 R. James, T. David and R. Kaushal, *J. Nanomed. Nanotechol.*, 2012, **3**.

11 T. Shimizu, T. Teranishi, S. Hasegawa and M. Miyake, *The Journal of Physical Chemistry B*, 2003, **107**, 2719.

12 S. V. Kumar and S. Ganesan, *International Journal of Green Nanotechnology*, 2011, **3**, 47.

13 D. Li and R. B. Kaner, *J. Am. Chem. Soc.*, 2006, **128**, 968.

14 A. Goel and N. Rani, *Open Journal of Inorganic Chemistry*, 2012, **2**, 67.

15 J. Singh, A. Roychoudhury, M. Srivastava, P. R. Solanki, D. W. Lee, S. H. Lee and B. D. Malhotra, *Nanoscale*, 2014, **6**, 1195.

16 K. Lu and C. S. Kessler, in *Synthesis and Processing of Nanostructured Materials: Ceramic Engineering and Science Proceedings*, John Wiley & Sons, Inc., 2008, pp. 1.

17 L. Upadhyaya, J. Singh, V. Agarwal, A. C. Pandey, S. Verma, P. Das and R. P. Tewari, *J. Polym. Res.*, 2014, **21**, 1.

18 J. An, Q. Luo, X. Yuan, D. Wang and X. Li, *J. Appl. Polym. Sci.*, 2011, **120**, 3180.

19 D. K. Božanić, L. V. Trandafilović, A. S. Luyt and V. Djoković, *React. Funct. Polym.*, 2010, **70**, 869.

20 R. Pauliukaite, M. E. Ghica, O. Fatibello-Filho and C. M. A. Brett, *Electrochim. Acta*, 2010, **55**, 6239.

21 B. R. Schroeder, M. I. Ghare, C. Bhattacharya, R. Paul, Z. Yu, P. A. Zaleski, T. C. Bozeman, M. J. Rishel and S. M. Hecht, *J Am Chem Soc*, 2014, **136**, 13641.

22 Z. Yu, R. M. Schmaltz, T. C. Bozeman, R. Paul, M. J. Rishel, K. S. Tsosie and S. M. Hecht, *J Am Chem Soc*, 2013, **135**, 2883.

23 C. Bhattacharya, Z. Yu, M. J. Rishel and S. M. Hecht, *Biochemistry*, 2014, **53**, 3264.

24 S. Malathi, M. D. Balakumaran, P. T. Kalaichelvan and S. Balasubramanian, *Adv. Mat. Lett.*, 2013, **4**, 933.

25 R. Seda Tı˘glı Aydın and P. Mehlika, *J. Nanomater.*, 2012, **2012**, 1.
26 J. L. Arias, *Molecules*, 2008, **13**, 2340.
27 Z. Chen, X. Zhang, H. Cao and Y. Huang, *Analyst*, 2013, **138**, 2343.
28 Anuj N. Mishra, Seema Bhadauria, Mulayam S. Gaur, Renu Pasricha and B. S. Kushwah, *International Journal of Green Nanotechnology: Physics and Chemistry*, 2010, **1**, 118.
29 Chandan Singh, Ritesh K. Baboota, Pradeep K. Naik and H. Singh, *Adv. Mat. Lett.*, 2012, **3**, 279.
30 L. Gwen, K. Imelda, D. Barry, C.-T. Adrienne, R. Llewellyn, F. Peter and G. Lisbeth, *Biomacromolecules*, 2007, **8**, 2533.
31 M. R. Kasaai, in *Chitin, Chitosan, Oligosaccharides and Their Derivatives: Biological Activities and Applications*, ed. S.-K. Kim, CRC press, Taylor & Francis group, U.S.A., 1st edn., 2011, pp. 149.
32 D. Lin, H. Chen, X. Yadong and J. Huangxian, *Biomacromolecules*, 2007, **8**, 1341.
33 S. Korkiatithaweechai, A. Pangdam, A. Ekgasit and N. M. Praphairaksit, International conference nanomaterials: Applications and properties, Sumy State University, Ukraine, 2012.
34 A. Anitha, K. P. Chennazhi, S. V. Nair and R. Jayakumar, *J. Biomed. Nanotechnol.*, 2012, **8**, 29.
35 K. A. Mohamed Anwar, M. M. Mohsen and M. G. Magdy, *J. Nanomed. Nanotechol.*, 2012, **3**.
36 H. Wolfgang, T. K. T. Nguyen, A. Jenny and G. F. David, *Anal. Chem.*, 2007, **79**, 4215.
37 H. Liu, F. Yang, Y. Zheng, J. Kang, J. Qu and J. P. Chen, *Water Res*, 2011, **45**, 145.
38 S.-X. Teng, S.-G. Wang, X.-W. Liu, W.-X. Gong, X.-F. Sun, J.-J. Cui and B.-Y. Gao, *Colloids Surf., A*, 2009, **340**, 86.
39 L. Zhao, J. Zhou, H. Chen, M. Zhang, Z. Sui and X. Zhou, *Korean J. Chem. Eng.*, 2010, **27**, 1412.
40 M. Karra-Chaabouni, I. Bouaziz, S. Boufi, A. M. Botelho do Rego and Y. Gargouri, *Colloids Surf., B*, 2008, **66**, 168.
41 A. Fraczek-Szczypta, E. Menaszek, T. B. Syeda, A. Misra, M. Alavijeh, J. Adu and S. Blazewicz, *J. Nanopart. Res.*, 2012, **14**, 1181.
42 A. Fraczek-Szczypta, E. Menaszek, T. Syeda, A. Misra, M. Alavijeh, J. Adu and S. Blazewicz, *J. Nanopart. Res.*, 2012, **14**, 1.
43 Y. Wang, B. Li, Y. Zhou, D. Jia and Y. Song, *Polym. Adv. Technol.*, 2011, **22**, 1681.
44 C. K. Lim and A. S. Halim, in *Biopolymers*, ed. E. Magdy M., Sciyo publisher, Croatia, 1st edn., 2010, pp. 209.
45 K. Szczepanowicz, J. Stefanska, R. P. Socha and P. Warszyn'ski, *Physicochem Probl Miner Process*, 2010, **45**, 85.
46 S. Shanmugam, B. Viswanathan and T. K. Varadarajan, *Nanoscale. Res. Lett.*, 2007, **2**, 175.
47 R. Prado-Gotor, G. López-Pérez, M. J. Martín, F. Cabrera-Escribano and A. Franconetti, *J Inorg Biochem*, 2014, **135**, 77.
48 D. Bhumkar, H. Joshi, M. Sastry and V. Pokharkar, *Pharm. Res.*, 2007, **24**, 1415.
49 A. Komalam, L. Muraleegharan, S. Subburaj, S. Suseela, A. Babu and S. George, *Int Nano Lett*, 2012, **2**, 1.
50 Z. Zhou, D. Cao, L. Liu, Q. Liu, Y. Zhao, W. Zeng, Q. Yi, Z. Yang and J. Zhou, *J. Macromol. Sci. B*, 2013, **52**, 973.

51 A. Anitha, K. P. Chennazhi, S. V. Nair and R. Jayakumar, *J. Biomed. Nanotechnol.*, 2012, **8**, 29.
52 P. R. Chandran and N. Sandhyarani, *RSC Advances*, 2014, **4**, 44922.
53 P. Montcourrier, I. Silver, R. Farnoud, I. Bird and H. Rochefort, *Clin Exp Metastasis*, 1997, **15**, 382.
54 M. Schindler, S. Grabski, E. Hoff and S. M. Simon, *Biochemistry*, 1996, **35**, 2811.
55 Y. Kato, S. Ozawa, C. Miyamoto, Y. Maehata, A. Suzuki, T. Maeda and Y. Baba, *Cancer Cell International*, 2013, **13**, 89.
56 F. Alexis, S. S. Venkatraman, S. K. Rath and F. Boey, *J. Controlled Release*, 2004, **98**, 67.
57 J. H. Jung, M. Park and S. Shinkai, *Chem. Soc. Rev.*, 2010, **39**, 4286.
58 Y. Ramgopal, S. S. Venkatraman and W. T. Godbey, *J. Appl. Polym. Sci.*, 2008, **108**, 659.

Figure captions

Figure 1. Schematic representing the preparation of 5-Fluorouracil loaded CS/Au nanocomposite.

Figure 2. XRD pattern of CS/Au nanocomposite containing various percentages of gold and 5-FU encapsulated nanocomposite.

Figure 3. FTIR spectra of CS/Au nanocomposite containing various percentages of gold.

Figure 4. FTIR spectra of 5-FU encapsulated CS/Au nanocomposite.

Figure 5. UV-VIS spectra of CS/Au nanocomposite containing various percentages of gold.

Figure 6. HRTEM image of CS/Au nanocomposite showing the (a) polymer matrix structure, (b) & (C) diffraction planes of gold, (d) & (e) HRTEM image of 5-FU encapsulated CS/Au nanocomposite showing the agglomeration of nanoparticles and increase in particle size, (f)Elemental mapping of 5-FU encapsulated CS/Au showing gold and 5-FU.

Figure 7. SAED pattern of (a) CS/Au nanocomposite, (b) 5-FU encapsulated CS/Au nanocomposite.

Figure 8. XPS of CS/Au nanocomposite (a) survey spectrum, (b) C-1s spectrum, (c) N-1s spectrum, (d) O-1s spectrum, (e) Au-4f spectrum.

Figure 9. Zeta potential of CS/Au nanocomposite

Figure 10. (a) Drug release profile of 5-FU encapsulated CS/Au nanocomposite, (b) Cytotoxity analysis of 5-FU encapsulated CS/Au nanocomposite towards MCF-7 and VERO cells.

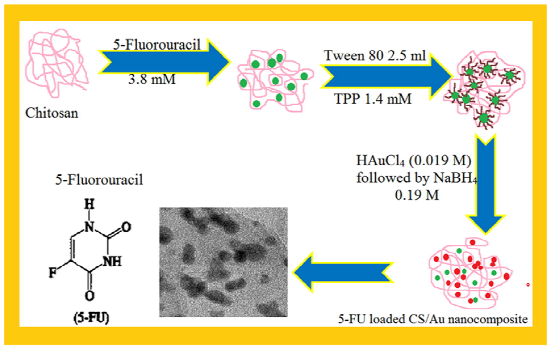

Figure 1

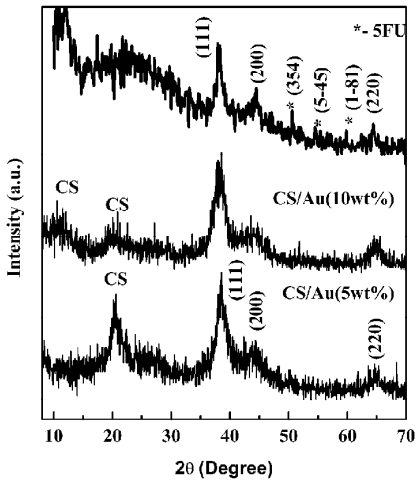

Figure 2

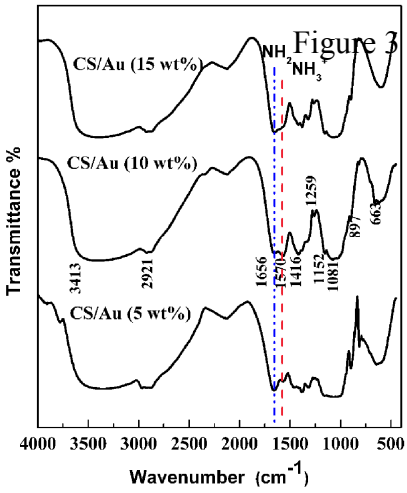

Figure 3

Figure 3

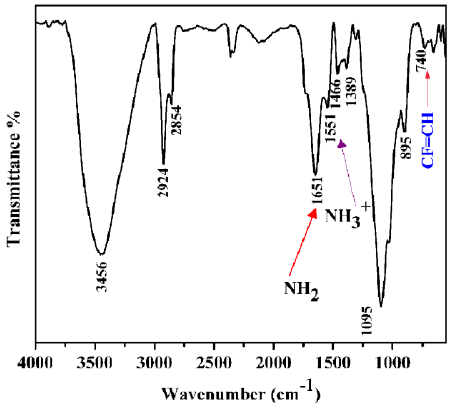

Figure 4

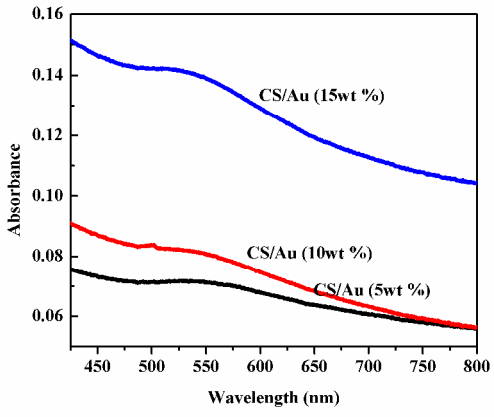

Figure 5

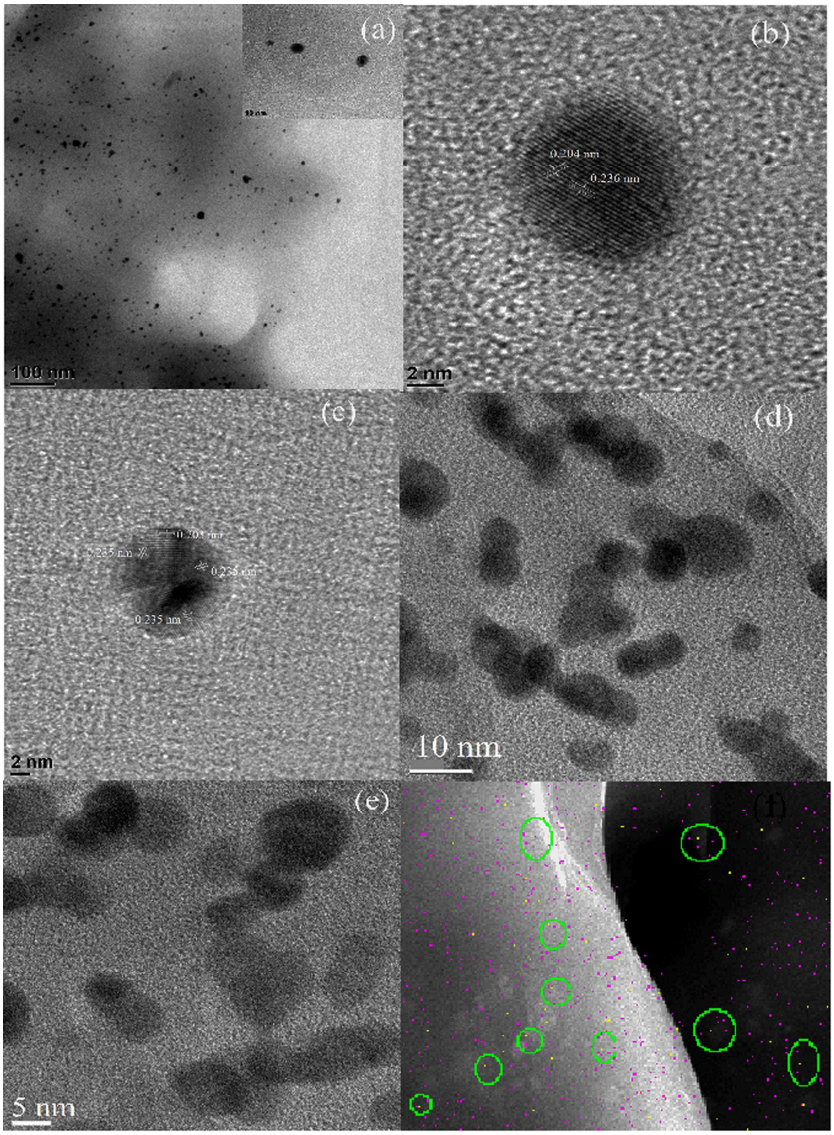

Figure 6

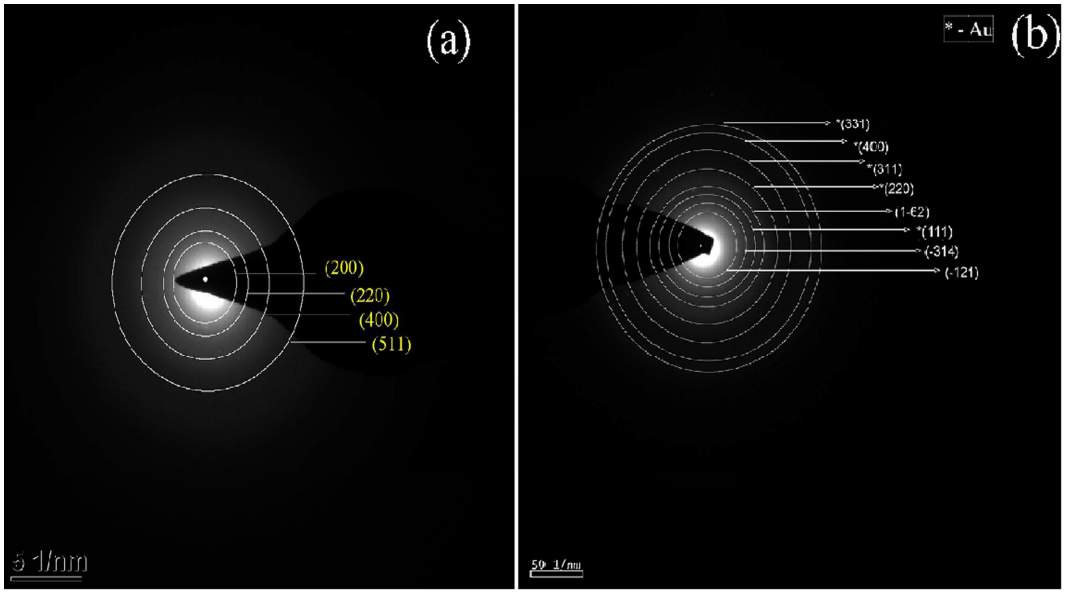

Figure 7

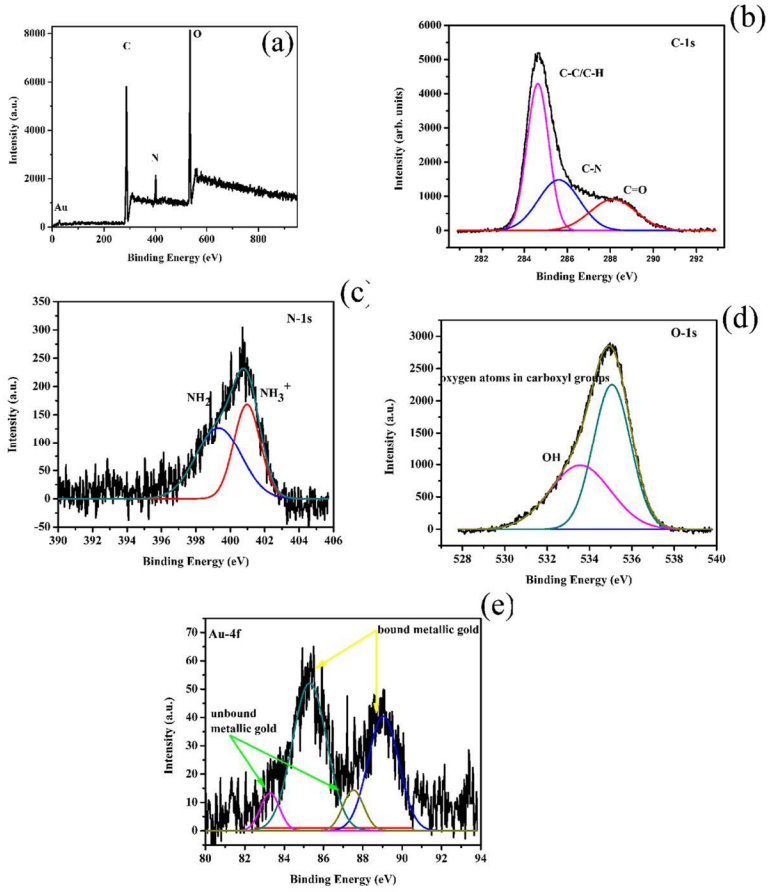

Figure 8

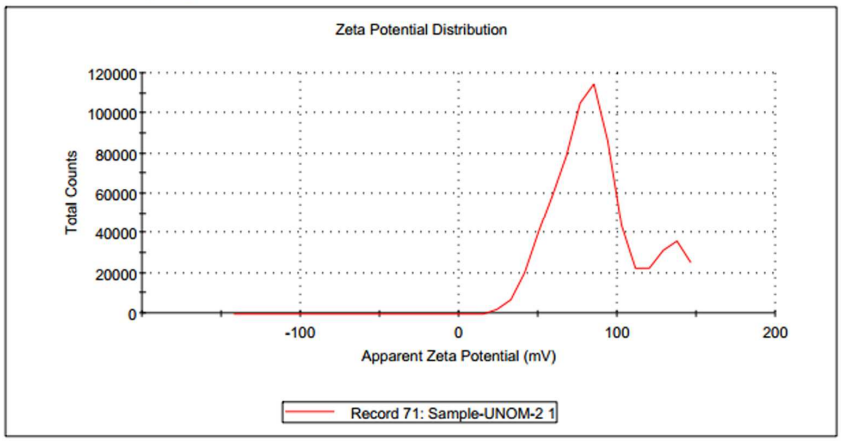

Figure 9

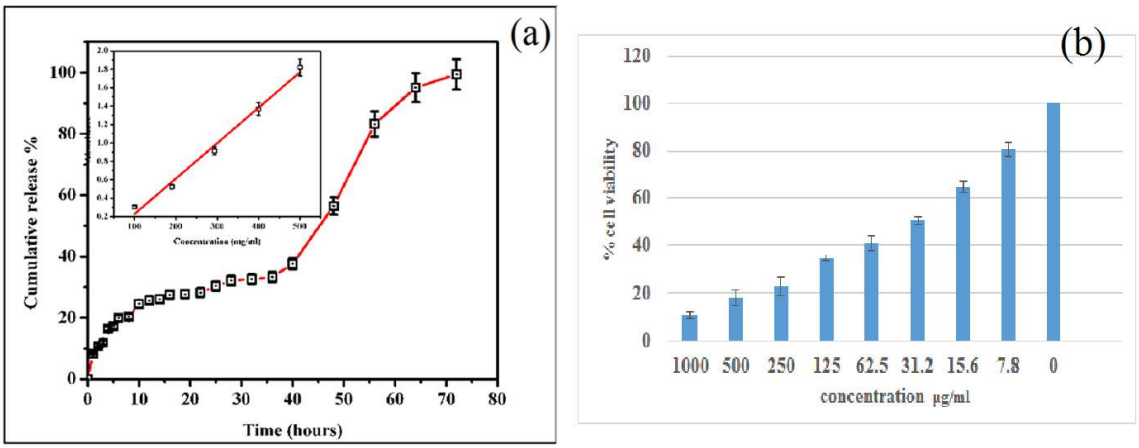

Figure 10